Proceedings of the 11th ICPMG 2026
11th International Conference on Physical Modelling in Geotechnics
8-12 June 2026, Zurich, Switzerland

Experimental evaluation of crushed stone backfill reaction behind concrete caissons under cyclic loading

O. Kurihara
Port and Airport Research Institute, Yokosuka, Japan, kurihara-oo@p.mpat.go.jp

H. Takahashi
Tokyo University of Marine Science and Technology, Tokyo, Japan, takahashi-h@kaiyodai.ac.jp

ABSTRACT: Concrete caisson structures founded on crushed stone mounds are widely used in Japan and have increasingly gained international recognition as effective coastal wave defence systems. However, recent damage caused by high waves and tsunamis has prompted renewed efforts to reinforce these structures. A commonly adopted reinforcement measure involves placing a crushed stone reinforcing embankment behind the caisson, which improves resistance against sliding, bearing capacity failure, and excessive toe pressure. Despite these developments, the overturning resistance of caissons remains insufficiently understood, mainly due to the limited knowledge of resistance mobilisation in crushed stone embankments under small rotational displacements and cyclic movements of the caisson. This study investigates the fundamental resistance characteristics of crushed stone reinforcing embankments against caisson rotation through centrifuge model tests using an inclined loading plate. The model test results demonstrate a distinctly nonlinear relationship between resistance force and inclination angle, with resistance behaviour strongly influenced by cyclic loading history. Under monotonic loading, the resisting moment increased with inclination angle, indicating that resistance continued to be mobilized at large rotations. In contrast, after exposure to large rotational loading, the resistance against smaller subsequent rotations decreased. These results highlight the importance of accounting for nonlinear and cyclic resistance characteristics when evaluating overturning stability of reinforced caisson structures.

1 INTRODUCTION

Concrete caisson structures founded on crushed stone mounds are widely used in Japan and have increasingly gained international recognition as effective coastal wave defence systems. Their widespread adoption stems from their proven performance under severe wave conditions and their long operational history along the Japanese coast. However, recent incidents of damage induced by high waves and tsunamis have highlighted the need for further reinforcement of these systems. In Japan, particularly following the 2011 Great East Japan Earthquake, extensive efforts have been made to improve the stability of composite-type breakwaters, leading to the growing application of crushed stone embankments placed behind caissons as a reinforcement measure.

These backfilling embankments have been shown to effectively mitigate several key failure modes, including sliding, bearing capacity failure, and excessive toe pressure (e.g., Takahashi, 2021). Corresponding design and verification methodologies for these failure mechanisms have been well established (e.g., MLIT et al., 2020). Moreover, previous studies have also examined catastrophic failure modes associated with composite breakwaters (e.g., Kurihara & Takahashi, 2023). Despite these advances, overturning—another critical failure mode—remains comparatively underexplored. This is due in part to the unique mechanics of overturning: unlike sliding or bearing capacity failure, which can often be assessed through external force equilibrium, overturning involves complex interactions between caisson rotation, deformation of the supporting rubble, and changes in the moment arm between the caisson heel and its centre of gravity. As the caisson rotates, the rubble embankment mobilizes reactive resistance through deformation, while the self-weight moment decreases due to geometric changes, complicating straightforward evaluation.

A major challenge in progressing overturning research lies in the limited understanding of how crushed stone embankments mobilize resistance against small rotational displacements and repeated cyclic movements—conditions that occur frequently under wave and tsunami loading. The mechanisms governing reactive force development in crushed stone, particularly under minor but cumulative rotational motions, have not been systematically clarified in previous studies.

To address this gap, the present study investigates the fundamental behaviour of resistance forces exerted by crushed stone embankments against rotational and cyclic movement of caissons. Centrifuge model tests were conducted using a tilting load plate capable of reproducing prototype-scale ground stress conditions, enabling controlled simulation of caisson rotation and cyclic loading. Through these tests, this study aims to provide foundational insights into the nonlinear and cyclic reactive characteristics of rubble embankments, thereby contributing to improved evaluation and design of overturning stability for reinforced composite-type breakwaters.

2 MODEL TEST SETUP

This study employed centrifuge model tests to investigate the fundamental resistance behaviour of crushed stone embankments subjected to rotational and cyclic movements of a caisson. The tests were conducted at a model scale of 1/30 under a centrifugal acceleration of 30*g*, enabling reproduction of prototype-level stress conditions within the ground. The centrifuge apparatus used in this study is the PARI Mark II-R hydro-geotechnical centrifuge. Details of the centrifuge can be found in Takahashi et al. (2019).

2.1 Model Layout and Test Container

Figure 1 shows the model test cross-section. A rigid soil container measuring 1.4 m in length, 0.6 m in height, and 0.2 m in width was used to construct the physical models. An inclined loading plate, representing the rear face of a caisson, was installed along one side of the container. The crushed stones used for the reinforcing embankment are shown in Figure 2. A crushed stone embankment composed of approximately 10 mm crushed stones was placed adjacent to the loading plate. In actual breakwater configurations, both the caisson and the embankment rest on a mound foundation. To replicate this condition while simplifying the model test configuration, the mound beneath the embankment and the embankment body were modelled using crushed stones in a medium-dense state, without differentiating between the two layers. The bottom supporting layer was constructed as a dense crushed stone layer to ensure stable boundary conditions. It should be noted that this study examines the

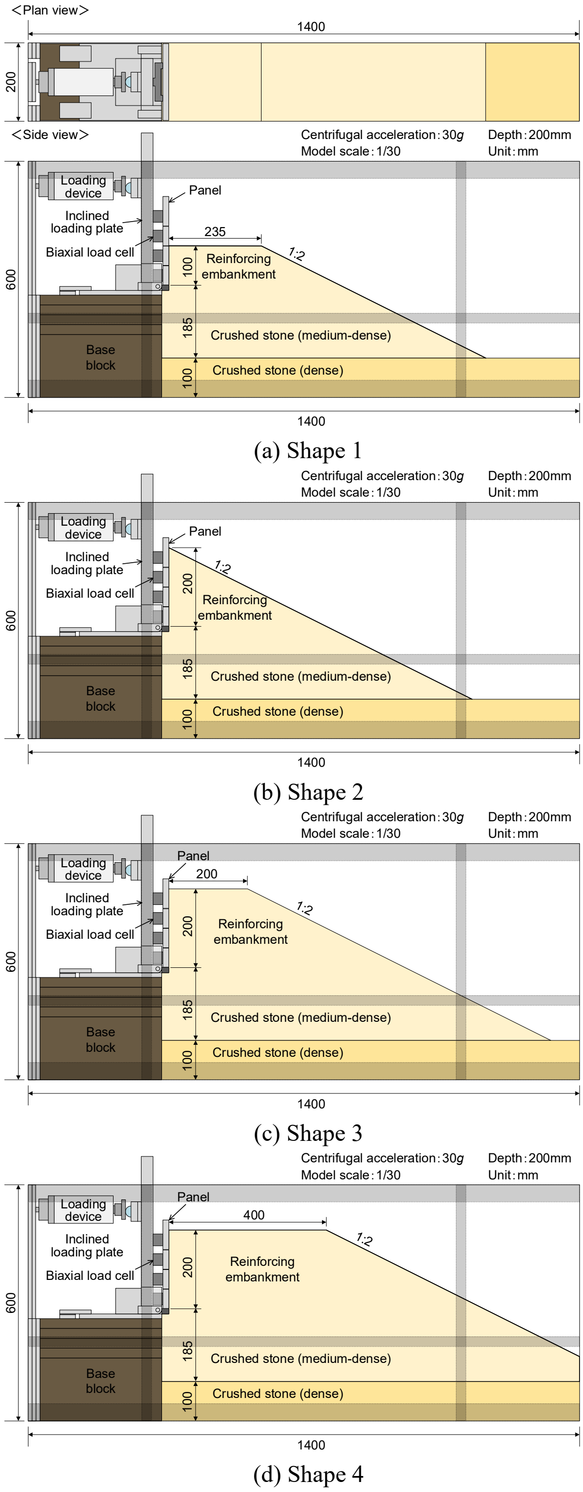

Figure 1. Model test cross-section.

Figure 2. 10 mm crushed stones used for the reinforcing embankment.

fundamental resistance behaviour due to the embankment configuration, and all cases were conducted under dry conditions for simplification.

2.2 Inclined Loading Plate and Instrumentation

The inclined loading plate (Figure 3) was hinged at its base and consisted of four stacked panels. A biaxial load cell was installed behind each panel to measure the reaction forces mobilized by the reinforcing embankment. The loading plate was tilted toward the embankment using a hydraulically driven horizontal loading device, thereby simulating the inclination and overturning motion of a caisson and enabling measurement of the resistance force exerted by the embankment.

The resisting moment generated by the embankment was calculated by multiplying the resistance force measured at each panel by the vertical distance from the lower edge of the panel to the corresponding load cell. The total resisting moment was obtained by summing the moments from all four panels. The effective lever arm (or application height) of the embankment resistance was then determined by dividing the total resisting moment by the total resistance force.

To prevent vertical constraint during rotation, the tip of the horizontal loading device was fitted with a circular plate, while the contact point on the inclined loading plate was equipped with a spherical roller, allowing relative movement at the contact interface during tilting (Figure 4). Due to the structural configuration of the inclined loading plate, the centre of rotation was slightly offset from the ideal heel of the caisson. As a result, the bottom edge of the plate experienced a very small horizontal displacement during rotation. However, this effect was negligible and did not influence the evaluation of the embankment resistance, as the horizontal displacement decreased towards the lower part of the plate.

2.3 Embankment Geometries and Loading Conditions

The model test conditions are summarized in Table 1. Four embankment geometries were examined by varying the height and crest width of the reinforcing embankment. Shapes 1 and 2 have identical cross-sectional areas but differ in height and crest width. Shape 2 is a triangular embankment with a height of 200 mm and a crest width of 0 mm, whereas Shape 1 is a trapezoidal embankment obtained by reducing the height of Shape 2 to 100 mm.

Shape 3 has the same height as Shape 2, with an increased crest width of 200 mm, and Shape 4 further increases the crest width to 400 mm. Shapes 3 and 4 were designed to investigate the influence of crest width on the resistance characteristics of the reinforcing embankment.

Two loading protocols were adopted. The first consisted of three loading cycles with a maximum inclination angle of 15° (15° × 3 cycles). The second

Figure 3. Inclined loading plate.

Figure 4. Inclined loading plate (left) and horizontal loading device (right).

Table 1. Model test conditions (values in parentheses indicate prototype scale).

Case	Embankment height	Embankment crest width	Embankment shape	Loading protocol
S1-L S1-C	100 mm (3 m)	235 mm (7 m)	Shape 1	15° × 3 cycles 0.5°, 1°, 2°, and 4° × 10 cycles each
S2-L S2-C	200 mm (6 m)	0 mm (0 m)	Shape 2	15° × 3 cycles 0.5°, 1°, 2°, and 4° × 10 cycles each
S3-L S3-C	200 mm (6 m)	200 mm (6 m)	Shape 3	15° × 3 cycles 0.5°, 1°, 2°, and 4° × 10 cycles each
S4-L S4-C	200 mm (6 m)	400 mm (12 m)	Shape 4	15° × 3 cycles 0.5°, 1°, 2°, and 4° × 10 cycles each

consisted of cyclic loading with maximum inclination angles of 0.5°, 1°, 2°, and 4°, with ten cycles applied at each angle. Each loading cycle comprised monotonic rotation to the specified maximum inclination angle, a holding period, and unloading back to the initial position. The angular velocity during both loading and unloading was kept constant at approximately 2.2°/min.

To illustrate the relationship between inclination angle and horizontal displacement at the caisson crest, a simple example is provided. For a caisson with a height of 10 m, the horizontal displacement of the crest is 2.68 m at an inclination angle of 15° (10 × tan 15°) and 0.17 m at an inclination angle of 1° (10 × tan 1°).

Based on this relationship, the large-angle loading tests with a maximum inclination of 15° were designed to evaluate the resistance behaviour of the embankment under conditions where caisson overturning progresses significantly, such as during extreme wave or tsunami events. In contrast, the cyclic loading tests with maximum inclination angles ranging from 0.5° to 4° were intended to represent the resistance behaviour of the embankment under repeated external loading near the allowable inclination range of actual caissons during ordinary wave conditions.

3 RESULTS OF LARGE-ANGLE LOADING (15° × 3 CYCLES)

3.1 Deformation Characteristics

The deformation characteristics of the crushed stone embankment were primarily assessed through visual observations of the test footage and photographs. Figure 5 shows the state of the embankment for Shape 3 before and after the 15° × 3-cycle loading. Based on these visual inspections, the entire embankment ground was seen to be mobilised during the initial loading cycle. The crushed stone embankment exhibited an upward and outward migration towards the slope and crest, forming a slightly heaved deformation pattern. Since the horizontal displacement of the inclined loading plate increased with height, the embankment showed a similar deformation trend, with larger horizontal displacements occurring in the upper part of the embankment.

Near the loading plate, the crushed stone was compacted by passive failure during the first loading cycle. However, during unloading, this same region loosened as a result of active failure. In the second loading cycle, the embankment material near the panel, which had loosened during the previous unloading, did not re-compact immediately. Instead, it gradually returned to a dense state only after the plate inclination had progressed to a relatively large angle, after which the deformation behaviour became similar to that of the first cycle. The third loading cycle exhibited deformation characteristics similar to the second.

Further visual analysis of the footage revealed that the crushed stone near the panel migrated horizontally with a slight upward heave during loading, which helped maintain the crest height of the embankment. In contrast, during unloading, the material collapsed towards the panel, leading to a reduction in the crest height, with more significant settlement occurring closer to the panel. The embankment ground away from the loading plate also exhibited horizontal movement accompanied by slight heaving during loading, followed by contraction of the heaved portion during the initial stage of unloading.

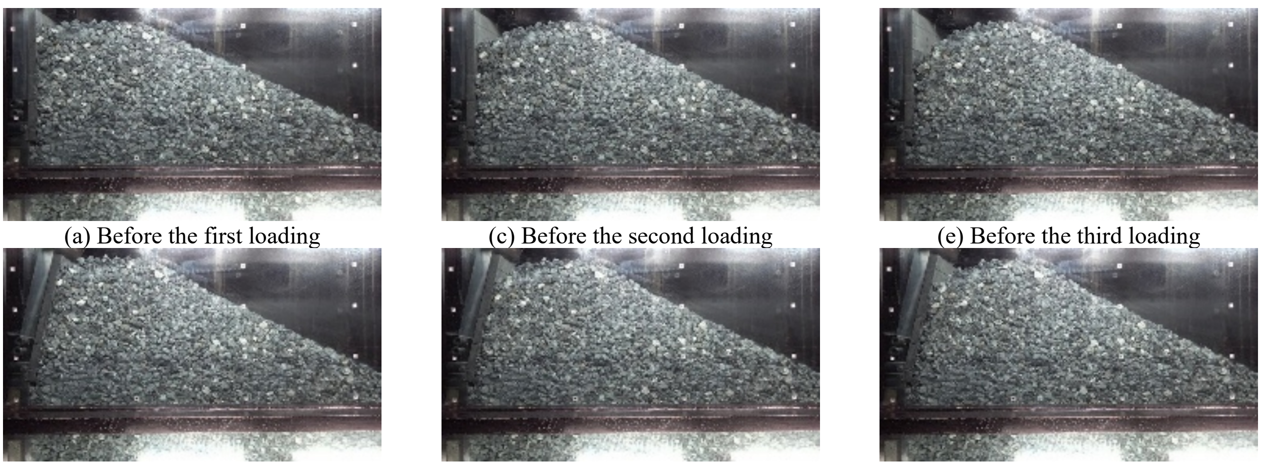

(a) Before the first loading (c) Before the second loading (e) Before the third loading

(b) After the first loading (d) After the second loading (f) After the third loading

Figure 5. Conditions before and after loading for Shape 3.

3.2 Resistance Characteristics under Large-Angle Loading

Figure 6 shows the relationships between the embankment resistance force, the resisting moment, the effective lever arm, and the inclination angle. The resistance force–inclination relationship exhibited pronounced nonlinearity throughout the loading cycles.

During the first loading cycle, the resistance force increased rapidly at small inclination angles, followed by yielding and a subsequent reduction in the slope of the curve. In contrast, during the second and subsequent cycles, the initial stiffness was smaller than that observed in the first cycle. This reduction can be attributed to loosening of the embankment material near the panel caused by active failure during unloading of the preceding cycle. As loading progressed, the resistance force increased again in the mid-stage of the cycle as the loosened material gradually returned to a dense state, after which yielding occurred. Consequently, the resistance–inclination relationship remained nonlinear in all cycles. With increasing number of cycles, the resistance force at the maximum inclination angle increased progressively.

The resisting moment generated by the embankment increased with inclination angle in a manner similar to the resistance force, indicating a sustained increase in resistance even at large rotations. However, although the resistance force at the maximum inclination increased with cycle number, the corresponding increase in resisting moment was relatively limited. This behaviour is attributed to a reduction in the effective lever arm caused by a decrease in embankment height near the panel, resulting from cumulative deformation during repeated loading. As a result, the effective lever arm during the second and third cycles was smaller than that during the first cycle.

Figure 7 compares the resisting moment–inclination relationships for Shapes 1 to 4, with emphasis on the 0°–1° inclination range in the first 15° loading cycle. A comparison between Shapes 1 and 2, which have the same cross-sectional area, indicates that concentrating the embankment volume closer to the caisson by increasing its height leads to higher initial stiffness and a larger resisting moment. Specifically, Shape 2, which has a greater height and places more material in direct contact with the upper part of the loading plate, exhibited superior resistance

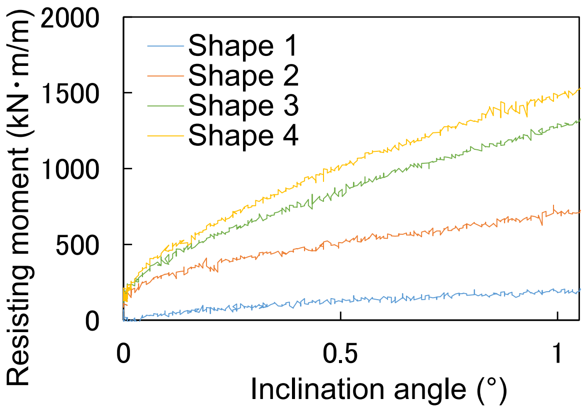

Figure 7. Enlarged comparison of resisting moment versus inclination angle for Shapes 1 to 4 in the 0°–1° range during the first 15° loading cycle.

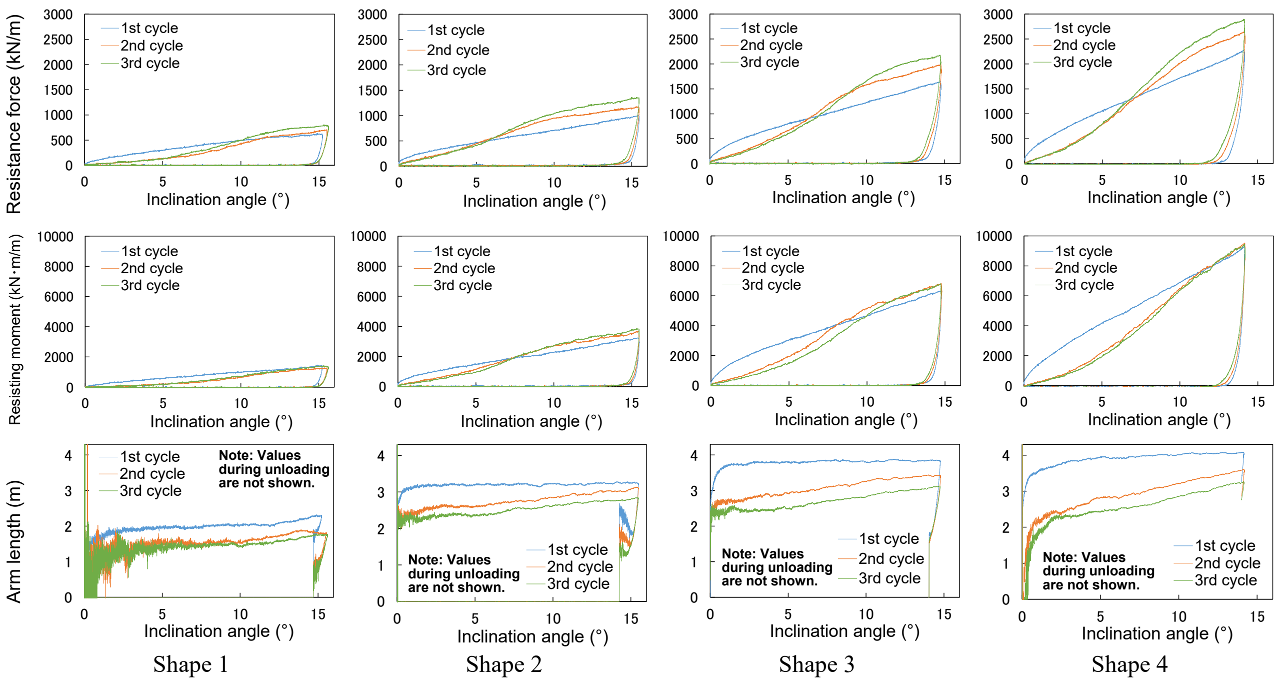

Figure 6. Resistance force, resisting moment, and arm length versus inclination angle (prototype scale).

compared to Shape 1. Furthermore, the comparison of Shapes 2, 3, and 4 shows that increasing the crest width further enhances the resistance force. However, the increase in resisting moment from Shape 3 to Shape 4 was smaller than that from Shape 2 to Shape 3, suggesting that the influence of crest width on the enhancement of initial stiffness and resisting moment diminishes as the width increases.

4 RESULTS OF CYCLIC LOADING TESTS

4.1 Deformation Characteristics under Cyclic Loading

Particle Image Velocimetry (PIV) analysis was performed using images captured before and after cyclic loading at each maximum inclination angle. Figure 8 shows the displacement of the reinforcing embankment before and after cyclic loading, where the background corresponds to the post-loading image. The deformation zone expanded in an arcuate pattern from the rotation centre toward the crest and slope of the embankment.

Repeated cycles of passive and active failure caused settlement of the embankment crest near the panel wall. During inclination, deformation increased with elevation along the loading plate; consequently, larger displacements were observed in the upper part of the embankment adjacent to the panel wall.

A comparison among Shapes 2 to 4 indicates that embankments with narrower crest widths exhibited larger deformation zones for the same displacement magnitude, implying greater mobility of the embankment material. In the case of the triangular embankment, deformation extended down to the slope at the elevation corresponding to the lower edge of the panel.

4.2 Resistance Characteristics under Cyclic Loading

Figure 9 shows the relationships between embankment resistance force, resisting moment, effective lever arm, and inclination angle under cyclic loading. In addition, Figure 10 presents stacked bar charts illustrating the moment at each inclination angle during cyclic loading and the inclination angle corresponding to each moment during cyclic loading.

Regarding the relationship between the resistance force and the inclination angle of the embankment, the initial loading in each stage (e.g. the 1st cycle at 4°) followed the stiffness slope observed at the end of the previous stage (e.g. the 10th cycle at 2°). As the inclination angle increased beyond the maximum angle of the preceding stage (e.g. 2°), the embankment ground began to yield, resulting in a reduction in the rate of resistance increase. Consequently, the relationship between the resistance force and the inclination angle of the embankment exhibited a distinctly nonlinear behaviour. During the

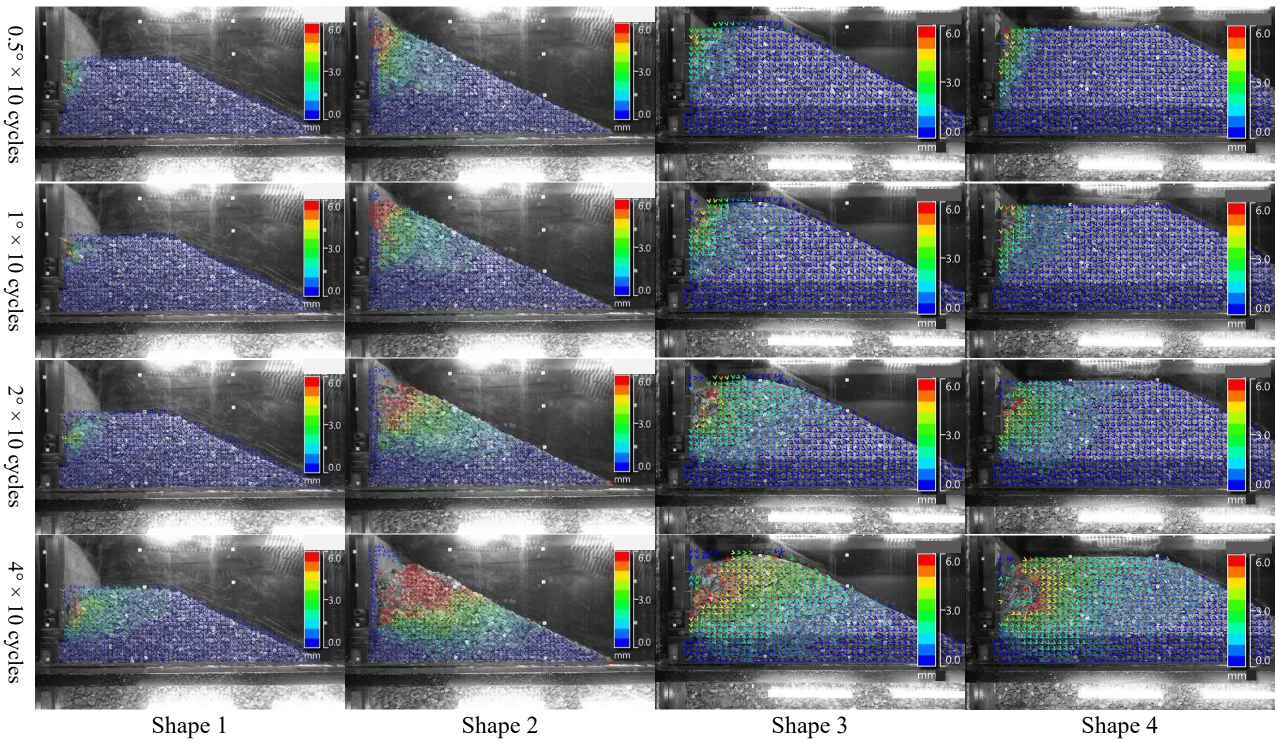

Figure 8. Displacement of the reinforcing embankment before and after cyclic loading (model scale).

initial stage of the second and subsequent cycles, the resistance force was smaller than that of the first cycle due to prior deformation; however, as loading progressed, the slope partially recovered and the resistance force exceeded that observed in the first cycle. These results indicate that once the embankment experiences loading at a large inclination angle, its resistance against smaller subsequent loads is reduced.

At the maximum inclination angle of each loading stage, the resistance force increased with the number of cycles. This trend was observed consistently for all four embankment shapes. For the same inclination angle, larger resistance forces were mobilized by embankments with greater height, and for embankments with the same height, by those with wider crest widths. In contrast, the effective lever arm of the resistance force decreased with increasing cycle number and with increasing maximum inclination angle.

The moment evaluated at each inclination angle during cyclic loading provides further insight into the resistance behaviour. For maximum inclination angles up to 2°, the resisting moment at the maximum inclination increased with cycle number. For example, considering Shape 2, if the resisting moment at 0.5° during the first cycle is used for design, repeated caisson rotations up to 0.5° result in an increase in the resisting moment at that inclination. When the caisson is repeatedly rotated up to 1°, the resisting moment at 0.5° decreases from the first to the second cycle but remains nearly constant thereafter, reaching a value comparable to that obtained in the first cycle at 0.5°. This suggests that, even when the inclination reaches up to twice the design value of 0.5°, the resisting moment

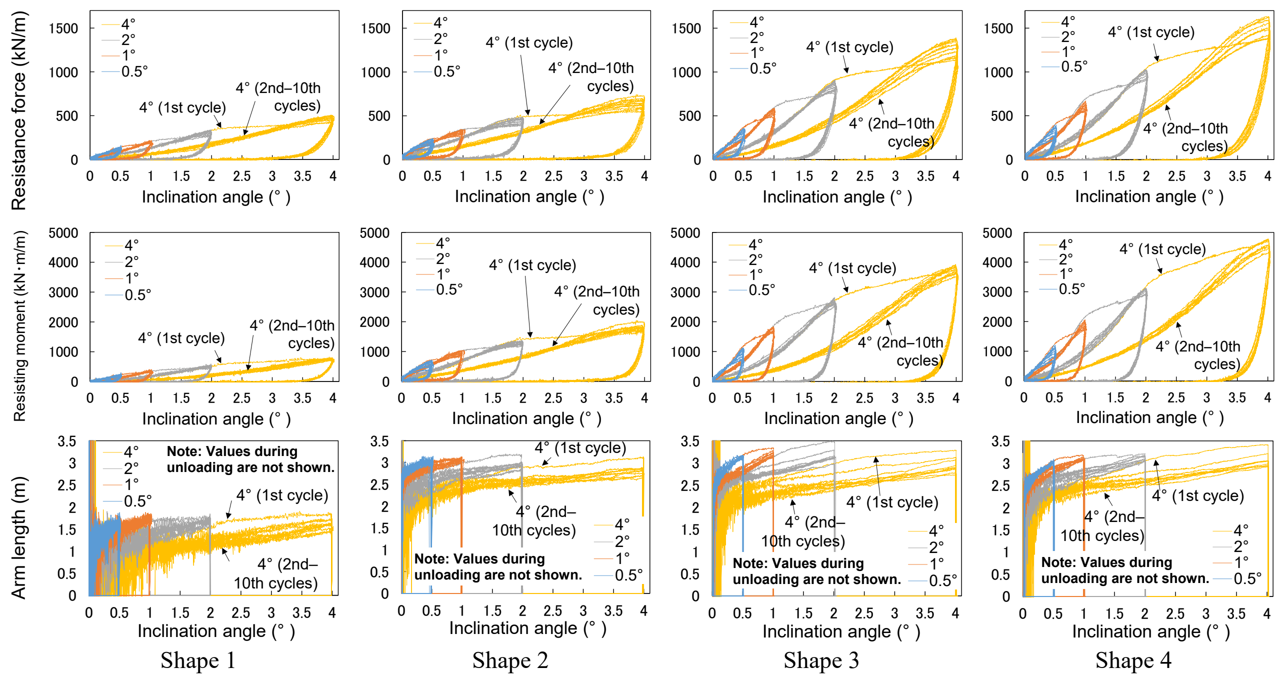

Figure 9. Resistance force, resisting moment, and arm length versus inclination angle (prototype scale).

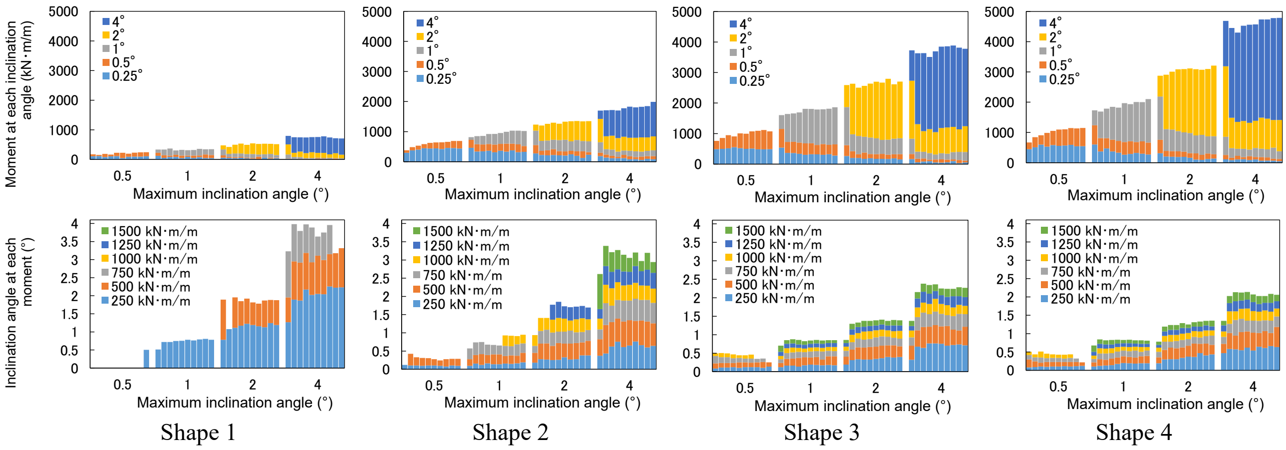

Figure 10. Moment at each inclination angle and inclination angle at each moment during cyclic loading (prototype scale).

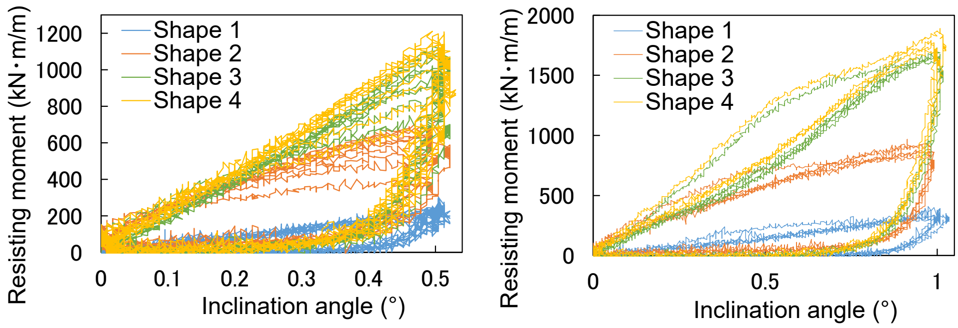

(a) 0.5° × 10 cycles (b) 1° × 10 cycles

Figure 11. Comparison of resisting moment versus inclination angle for Shapes 1 to 4 under cyclic loading.

corresponding to 0.5° can be maintained. Accordingly, the moment evaluated at specific inclination angles during cyclic loading can serve as a useful indicator for assessing embankment resistance.

Conversely, examination of the inclination angle corresponding to a given moment during cyclic loading reveals how the deformation capacity evolves. As shown in Figure 10, for loading stages with maximum inclination angles of 1° or greater, the inclination angle at which a moment of 500 kN·m/m was reached remained the same in the first cycle as in the preceding tenth cycle. However, from the second cycle onward, the inclination angle corresponding to the same moment increased, reflecting changes in the resistance–inclination relationship due to accumulated deformation.

Figure 11 compares the resisting moment–inclination relationships for Shapes 1 to 4 under cyclic loading, where Figure 11(a) corresponds to 0.5° × 10 cycles and Figure 11(b) to 1° × 10 cycles. Significant differences in initial stiffness and resisting moment are observed among Shapes 1, 2, and 3 due to variations in embankment height and crest width. In contrast, the difference between Shapes 3 and 4 is relatively small, indicating that under cyclic loading at small inclination angles such as 0.5° and 1°, increasing the crest width beyond a certain level yields diminishing improvement in resistance.

5 CONCLUSIONS

This study investigated the fundamental resistance characteristics of crushed stone reinforcing embankments during caisson overturning through static loading tests conducted in a centrifuge environment.

Centrifuge model tests demonstrated that the resistance force–inclination relationship of crushed stone reinforcing embankments is highly nonlinear and strongly influenced by loading history. Initial stiffness decreased after prior large rotations but partially recovered during subsequent loading as the embankment densified.

Under monotonic loading, the resisting moment generated by the embankment increased with increasing inclination angle, indicating that resistance continued to be mobilized even at large rotations. In contrast, under repeated loading, cumulative deformation near the loading plate reduced the effective lever arm, limiting the increase in resisting moment despite higher resistance forces.

Cyclic loading revealed a history-dependent response in which resistance against small rotations decreased after exposure to larger rotations, while resistance at the maximum inclination of each loading stage increased with cycle number.

Embankment geometry significantly affected resistance characteristics: increasing embankment height enhanced initial stiffness and resisting moment, whereas increasing crest width was effective only up to a certain level, beyond which further widening resulted in little additional improvement in resistance under small-angle cyclic loading.

These results indicate that overturning assessment of caisson–embankment systems must explicitly account for nonlinear resistance mobilisation and cyclic loading effects, as observed in the present model tests.

REFERENCES

Kurihara, O. and Takahashi, H. (2023). Backfilling configuration to improve tenacity of composite-type breakwaters. *Coastal Engineering Journal*, Vol. 65, Issue 2, pp. 217-233. https://doi.org/10.1080/21664250.2023.2167502

Ministry of Land, Infrastructure, Transport and Tourism (MLIT), National Institute for Land and Infrastructure Management (NILIM), and Port and Airport Research Institute (PARI). (2020). Technical Standards and Commentaries for Port and Harbour Facilities in Japan.

Overseas Coastal Area Development Institute of Japan, 2182p.

Takahashi, H. (2021). Stability of composite-type breakwaters reinforced by rubble embankment. *Soils and Foundations*, Vol. 61, Issue 2, pp. 318-334. https://doi.org/10.1016/j.sandf.2020.10.011

Takahashi, H., Fujii, N., Morikawa, Y., and Takano, D. (2019). Development of hydro-geotechnical centrifuge PARI Mark II-R. *Technical Note of the Port and Airport Research Institute*, No. 1353, 27p.